Mutation of plasma membrane Ca^{2+} ATPase isoform 3 in a family with X-linked congenital cerebellar ataxia impairs Ca^{2+} homeostasis

Ginevra Zanni[a,1], Tito Cali[b,1], Vera M. Kalscheuer[c], Denis Ottolini[d], Sabina Barresi[a], Nicolas Lebrun[e], Luisa Montecchi-Palazzi[f], Hao Hu[c], Jamel Chelly[e], Enrico Bertini[a,2], Marisa Brini[b,2], and Ernesto Carafoli[g,2]

[a]Unit of Molecular Medicine for Neuromuscular and Neurodegenerative Disorders, Department of Neurosciences, Bambino Gesù Children's Hospital, Istituti di Ricovero e Cura a Carattere Scientifico (IRCCS), 00165 Rome, Italy; [b]Department of Comparative Biomedicine and Food Science, University of Padova, 35131 Padua, Italy; [c]Max Planck Institute for Molecular Genetics, Department of Human Molecular Genetics, D-14195 Berlin, Germany; [d]Department of Biomedical Sciences, University of Padova, 35131 Padua, Italy; [e]Department of Genetic and Development, Institut Cochin, Université Paris Descartes, Centre National de la Recherche Scientifique (CNRS), Unité Mixte de Recherche (UMR) 8104, 75014 Paris, France; [f]European Bioinformatics Institute (EBI), Wellcome Trust Genome Campus, Hinxton, Cambridge CB10 1SD, United Kingdom; and [g]Venetian Institute for Molecular Medicine, 35129 Padua, Italy

Edited by Gottfried Schatz, University of Basel, Reinach, Switzerland, and approved July 24, 2012 (received for review May 3, 2012)

Ca^{2+} in neurons is vital to processes such as neurotransmission, neurotoxicity, synaptic development, and gene expression. Disruption of Ca^{2+} homeostasis occurs in brain aging and in neurodegenerative disorders. Membrane transporters, among them the calmodulin (CaM)-activated plasma membrane Ca^{2+} ATPases (PMCAs) that extrude Ca^{2+} from the cell, play a key role in neuronal Ca^{2+} homeostasis. Using X-exome sequencing we have identified a missense mutation (G1107D) in the CaM-binding domain of isoform 3 of the PMCAs in a family with X-linked congenital cerebellar ataxia. PMCA3 is highly expressed in the cerebellum, particularly in the presynaptic terminals of parallel fibers–Purkinje neurons. To study the effects of the mutation on Ca^{2+} extrusion by the pump, model cells (HeLa) were cotransfected with expression plasmids encoding its mutant or wild-type (wt) variants and with the Ca^{2+}-sensing probe aequorin. The mutation reduced the ability of the PMCA3 pump to control the cellular homeostasis of Ca^{2+}. It significantly slowed the return to baseline of the Ca^{2+} transient induced by an inositol-trisphosphate ($InsP_3$)-linked plasma membrane agonist. It also compromised the ability of the pump to oppose the influx of Ca^{2+} through the plasma membrane capacitative channels.

calcium dysregulation | plasma membrane calcium pumps | isoforms | X-linked ataxia | cerebellar atrophy

The tight regulation of cell Ca^{2+} is crucial for neuronal development, function, and survival. The free Ca^{2+} level of neurons at rest is four orders of magnitude lower than in the external medium. Ca^{2+} coming from outside or from cellular stores regulates neuronal processes like excitability, neurotransmitter release, synaptic efficacy, and gene expression. The plasma membrane Ca^{2+} ATPases (PMCAs) cooperate with the Na^+/Ca^{2+} exchangers of the plasma membrane (NCX), the endoplasmic reticulum (ER) Ca^{2+}-ATPases (SERCA pumps), and the mitochondrial Ca^{2+} uptake system in counteracting the transient Ca^{2+} increases produced by neuronal stimulation by the influx of Ca^{2+} through voltage- and ligand-gated plasma membrane channels, the ER inositol-trisphosphate receptor ($InsP_3R$), and the ryanodine receptor (RyR) channels, and through the mitochondrial Ca^{2+} release system(s) (1). PMCA isoforms in mammals are the products of 4 separate genes, and the number of variants is increased to over 30 by alternative splicing of mRNAs, which affects the first cytosolic loop of the pump (site A) and its C-terminal tail (site C). The splicing variants are cell-specific and undergo regulation during cell development and differentiation. PMCAs consist of 10 transmembrane domains, 2 large intracellular loops, and N- and C-terminal cytoplasmic tails. The C-terminal tail contains the regulatory calmodulin (CaM)-binding domain, which interacts with two sites in the two cytosolic loops of the pump autoinhibiting the pump at rest: CaM displaces the domain from the two sites restoring full pump activity (2, 3). PMCA1 and PMCA4 are expressed in most tissues, and PMCA2 and PMCA3 are expressed predominantly (but not exclusively) in the brain: most neurons express the four basic PMCA isoforms and multiple splice variants. In the molecular cell layer of the cerebellum, PMCA2 and PMCA3 concentrate in synaptic regions [parallel excitatory fiber (PF)–Purkinje neuron (PN) synapse] with a complementary distribution: high levels of PMCA3 are associated with the axon terminals of granule cells (PF terminals/presynaptic side), whereas PMCA2 is most abundant in PN dendrites (PN-postsynaptic side). During development, the up-regulation of PMCA2 and -3 in dendrites and dendritic spines coincides with their maturation, reflecting the importance of the proper spatial organization of Ca^{2+}-extrusion systems for synaptic formation (4, 5). Studies on PMCA3 are much scarcer than those on the other three basic isoforms. Its gene, for instance, has never been knocked out, suggesting that the isoform might be essential to the early development of the embryo. Six alternatively mRNAs have been described for PMCA3 at splice site C, but only the *a* variant, which is C-terminally truncated as a result of the loss of the ORF caused by the insert, and the *b* unspliced variant were found in significant levels in rat brain (6). Genetic defects of neuronal Ca^{2+} homeostasis have been associated with diverse disease phenotype. For instance, defective Ca^{2+} influx in PNs has been linked to the overt ataxia of tottering mouse (7, 8). To date, genetic defects of PMCAs have been demonstrated only for PMCA2 [refs. 9, 10; for a review, see ref. 1): they generate deafness, which, however, is not the only disease phenotype caused by a PMCA2 pump defect. The Wriggle Sagami ataxic mouse, in which the development of the PN dendritic tree is impaired, and synaptic connections of PF on PN dendrites are decreased with malformed synaptic boutons, also had a defective *PMCA2* gene (11). Deafness in the *pmca2* KO mice has also been associated with an ataxic phenotype in which PNs show shrunken dendrites and reduced firing frequency attributable to a K^+ current driven by extraresidual Ca^{2+}, which prevents the regeneration of the action potential. Basal Ca^{2+} levels in these neurons are high, and the Ca^{2+} recovery kinetics slow: reduced Ca^{2+} clearance attributable to a PMCA pump defect perturbs Ca^{2+} dynamics in PN dendrites and disrupts the accuracy of cerebellar processing and motor coordination (12).

Next-generation sequencing (NGS) has revealed a missense mutation of the X-linked PMCA3 pump gene *ATP2B3* (GenBank accession no. NM_001001344) in a family with congenital cerebellar atrophy and normal cognitive development (13). The

Author contributions: G.Z., E.B., M.B., and E.C. designed research; T.C., D.O., and H.H. performed research; V.M.K., L.M.-P., and J.C. contributed new reagents/analytic tools; G.Z., T.C., S.B., N.L., E.B., M.B., and E.C. analyzed data; and G.Z., M.B., and E.C. wrote the paper.

The authors declare no conflict of interest.

This article is a PNAS Direct Submission.

[1]G.Z. and T.C. contributed equally to this work.

[2]To whom correspondence may be addressed. E-mail: enricosilvio.bertini@opbg.net, marisa.brini@unipd.it, or ernesto.carafoli@unipd.it.

This article contains supporting information online at www.pnas.org/lookup/suppl/doi:10.1073/pnas.1207488109/-/DCSupplemental.

mutation affects a conserved residue in the CaM-binding domain. We have analyzed the consequences of the mutation on the function of the pump by overexpressing constructs encoding its mutated full-length (*b*) and C-terminally truncated variants (*a*) in model cells. The results have shown that the mutated pump has a reduced ability to extrude Ca^{2+} from the cell.

Results

Identification of the ATP2B3/PMCA3 Mutation by X-Exome Sequencing. To identify the disease-causing mutation in the family with X-linked cerebellar ataxia (Fig. 1*A*) (13), we have performed massive parallel sequencing of the X-chromosome–specific exons using DNA of the index patient (III:1). After sequence analysis using in-house–developed tools and filtering against public databases (dbSNP; 185 genomes from the 1000 Genome Project), 200 Danish control individuals (14) and our database, 4 nonsynonymous variants remained: chrX:85169199A > G, chrX:111909355C > T, chrX:135782152A > G, and chrX:152483733G > A [base pair positions according to the National Center for Biotechnology Information (NCBI) 36/hg18 assembly of the human genome]. Subsequent Sanger sequencing in all family members indicated that only one of the changes, chrX:152483733G > A, cosegregated with the disease. Fig. 1*B* shows the sequencing results for a control, the index patient (III:1) and his mother (II:2). The mutation, c.3321G > A, is located in exon 20 of the *ATP2B3*/*PMCA3* gene (GenBank accession no. NM_001001344) and replaces a conserved Gly by Asp (p.G1107D) in the CaM-binding domain.

Comparative Analysis of Ca^{2+} Transport of the Overexpressed Full-Length and Truncated Wild-Type and Mutant Pump. Ca^{2+} transport by the PMCA3 pump was first monitored in control and patient-derived fibroblasts transfected with the plasmid encoding the Ca^{2+}-sensing probe aequorin targeted to the cytoplasm [cytAEQ (15)]. Even if fibroblasts express very small amounts of the full-length pump, and nearly undetectable levels of its C-terminally truncated version, experiments were still performed on possible effects of the PMCA3 mutation on Ca^{2+} homeostasis. As expected, the analysis failed to reveal differences (Fig. S1; see *SI Materials and Methods* for details). Thus, to explore the effect of the G1107D replacement on Ca^{2+} export by the PMCA3 pump, we generated the mutation in the human full-length (*b*) and in the splice (*a*) truncated variants of PMCA3 by site-directed mutagenesis (the splicing insert replaces the C-terminal 10 residues of the CaM-binding domain) (Fig. 2*A*). The occurrence of the G1107D mutation was verified by sequencing. The expression vectors were transfected in HeLa cells, and the cellular localization of the overexpressed pumps was assessed by immunocytochemistry. Fig. 2*B* shows that all pump variants were correctly targeted to the plasma membrane: the mutation, at least in model cells (most likely in the cerebellar neurons as well), did not affect their membrane sorting. Western blot analysis showed bands at the expected molecular mass of 135 kDa for the *b* and of 129 kDa for the *a* variant (Fig. 2*C*). The 250-kDa PMCA3 pump dimer was also visible (a total cell lysate from mock-transfected cells was loaded for comparison). A PMCA3 isoform–specific antibody and the 5F10 antibody that recognizes all isoforms revealed similar expression levels for the wild-type (wt) and the G1107D variants. HeLa cells were then cotransfected with expression plasmids for the pumps and for the cytosolic Ca^{2+}-sensing photoprotein aequorin (cytAEQ) and stimulated with the $InsP_3$-linked agonist histamine, to induce Ca^{2+} release from the ER and subsequent Ca^{2+} influx from the extracellular ambient. In agreement with previous findings (16), Fig. 3 *A* and *B* shows that cells overexpressing the PMCA3 pump had enhanced ability to clear the stimulation-induced Ca^{2+} transient: its height, both in the truncated (Fig. 3*C*) or full-length (Fig. 3*D*) variant, was lower than in control cells transfected only with cytAEQ. The micromolar cytosolic Ca^{2+} peaks values were: 3.57 ± 0.06 ($n = 14$) for cytAEQ; 2.64 ± 0.1 ($n = 12$) for wt PMCA3*b;* and 2.69 ± 0.05 ($n = 12$) for wt PMCA3*a*. No differences in the peak height were found in the cells overexpressing the mutant pump with respect to those overexpressing the wt PMCA3 [2.77 ± 0.05 ($n = 12$) for the PMCA3*a* G1107D; and 2.80 ± 0.06 ($n = 12$) for the corresponding PMCA3*b* G1107D), i.e., the G1107D mutation failed to affect the ability of PMCA3 to control the amplitude of the transients. The kinetics of the posttransient declining phase, which is an important index of the longer-term Ca^{2+} extrusion ability of the overexpressed PMCA pump, would, in principle, also be shaped by the activity of the SERCA pump, but separate experiments and previous work with SERCA pump inhibitors had shown that under the PMCA pump overexpression conditions used, the SERCA pump contribution was essentially irrelevant. At variance with what observed on the peak amplitude, the kinetics of the declining of the Ca^{2+} curves showed a delay for the mutant pump (Fig. 3 *A* and *B*, light and dark gray traces): these differences were quantified by calculating the mean slope of the tangent at the time of the half-decay peak (Fig. 3 *E* and *F*). The Ca^{2+} extrusion by the mutated pump was evidently decreased more prominently in the truncated form (Fig. 3*E*). The insets show mean values of the half-peak decay in seconds ± SEM: 14.17 ± 0.72 ($n = 18$) for cytAEQ, 11.79 ± 0.34 ($n = 19$) for the wt PMCA3*a*, 16.55 ± 0.48 ($n = 20$) for the G1107D PMCA3*a* ($P < 0.001$); and 13.89 ± 0.34 ($n = 19$) for the wt PMCA3*b* and 15.85 ± 0.48 ($n = 20$) for the G1107D PMCA3*b* ($P < 0.01$). Thus, the G1107D mutation induced a more prolonged retention of Ca^{2+} within the cytoplasm.

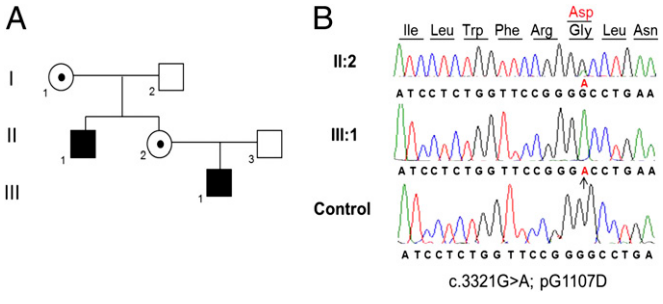

Fig. 1. Pedigree of the X-linked congenital ataxia family and mutation in *ATP2B3*. (*A*) Pedigree of the family with two affected males in different sibships suggesting X-linked inheritance. (*B*) Partial *ATP2B3* Sanger sequence chromatograms are shown for a normal control (*Bottom*), the index patient (III:1) (*Middle*), and his mother (II:2) (*Top*). The mutated amino acid change is shown on top. The mutated nucleotide in the index patient is marked by an arrow. *ATPB3* cDNA mutation is annotated according to human sequence GenBank accession no. NM_001001344, where +1 corresponds to the A of the ATG translation initiation codon.

Effect of the G1107D Mutation on the Response of PMCA3 to Ca^{2+} Entering Through the Capacitative Channels. The Ca^{2+} transients generated by the histamine stimulation under physiological concentrations of extracellular Ca^{2+} (1 mM $CaCl_2$) were the combined result of the Ca^{2+} released from the cellular stores (ER and Golgi) and of the Ca^{2+} influx from the external medium through the store-operated Ca^{2+} channels activated by their emptying (SOCE). To separately visualize the two components and to assess the effects of the overexpressed pumps on them, Ca^{2+} was first monitored in cells exposed to histamine in the absence of Ca^{2+} (i.e., in a medium containing 100 μM EGTA): the Ca^{2+} transient under these conditions was only shaped by the release of Ca^{2+} from the stores (first peak). The subsequent addition of 2 mM $CaCl_2$ induced a second transient, which represented the influx of the cation from the extracellular medium (second peak). A typical experiment with this protocol is reported in Fig. 4, in which the effect of the overexpression of the G1107D mutation in the *a* (Fig. 4 *A* and *B*) and in the *b* (Fig. 4 *C* and *D*) variants of the pump on the transients was analyzed. In agreement with the results in Fig. 3, the truncated and the full-length wt and G1107D pumps reduced the height of the first Ca^{2+} transient in a similar way [first peak values in μM ± SEM were: 2.11 ± 0.09 ($n = 9$) for cytAEQ; 1.53 ± 0.15 ($n = 9$) for the wt PMCA3*a*; 1.71 ± 0.11 ($n = 9$) for G1107D PMCA3*a*; 1.52 ± 0.1 ($n = 10$) for wt PMCA3*b*; 1.49 ± 0.08 ($n = 9$) for the G1107D PMCA3*b*]. Possibly, this was attributable to the

GENETICS

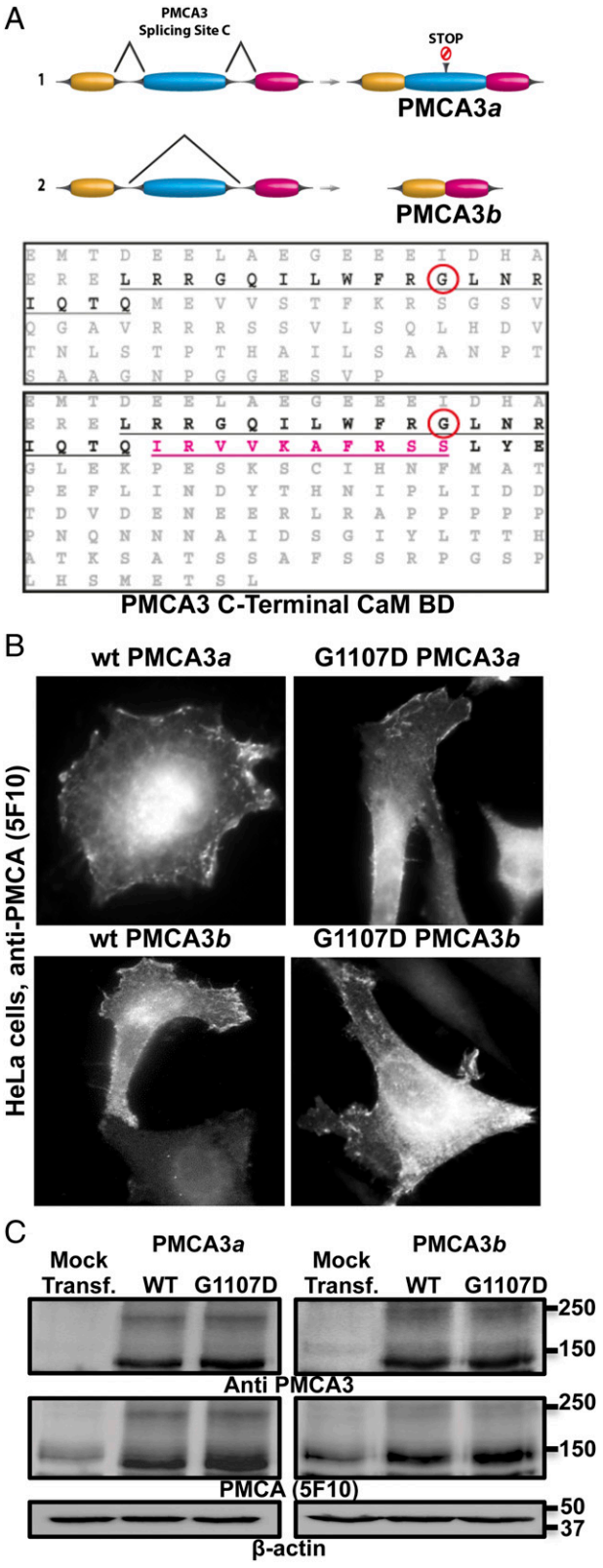

Fig. 2. Alternative splicing mechanism of PMCA3 at site C and analysis of the expression of exogenous PMCA3 variants in HeLa cells. (*A*) The numbers 1 and 2 indicate the splicing positions. The insertion of an exon generates a premature stop codon, leading to the formation of truncated isoform *a*. In 2, the pale blue exon is removed originating the full-length *b* isoform. The sequences of the two alternative C-terminal CaM binding domains generated by the splicing are shown in the right inbox of *A*. (*B* and *C*) Immunocytochemistry (*B*) and Western blot (*C*) analysis of PMCA3 distribution and expression level in HeLa cells expressing wt and mutant PMCA3 constructs. The PMCA3 was revealed by the 5F10 and the anti-PMCA3–specific antibody.

reduced ER Ca^{2+} content upon PMCA3 pump overexpression, an effect previously documented for the PMCA4 (17) and PMCA2 (18) isoforms and as confirmed in Fig. S2. Interestingly, however, the height of the peak generated by Ca^{2+} influx through the SOCE channels (second peak) was clearly reduced in the cells overexpressing the *a* (Fig. 4*B*) and the *b* (Fig. 4*D*) wt pump with respect to control cells but not in those overexpressing the mutant variants [in Fig. 4*B*, second peak values in μM ± SEM were: 2.00 ± 0.29 ($n = 8$) for cytAEQ, 1.48 ± 0.09 ($n = 8$) for the wt PMCA3*a*, 1.98 ± 0.11 ($n = 8$) for the G1107D PMCA3*a* ($P < 0.01$); and in Fig. 4*D*, the second peak values in μM ± SEM were: 1.65 ± 0.07 ($n = 7$) for the wt PMCA3*b*, 2.00 ± 0.17 ($n = 6$) for the G1107D PMCA3*b* ($P = 0.05$)]. The Ca^{2+} measurements confirmed that the *a* variant was more severely affected by the mutation than the *b* variant. The rate of the declining phase from the second (SOCE) transient was calculated at the mean half-decay time from the peak. No differences were detected between the mutant and wt forms [time for half-peak: 43.89 ±4.6 s ($n = 9$) for wt PMCA3*a*; 41.88 ± 3.84 ($n = 8$) for G1107D PMCA3*a*; 32.57 ± 3.19 ($n = 7$) for wt PMCA3*b*; and 39.14 ± 2.58 ($n = 7$) for the G1107D PMCA3*b*]. However, the calculation of the average Ca^{2+} values after 55 s (at the end of the trace) revealed higher values for the mutant variants [basal values in μM ± SEM were: 0.92 ± 0.05 ($n = 8$) for cytAEQ, 0.71 ± 0.05 ($n = 7$) for the wt PMCA3*a*, 0.95 ± 0.06 ($n = 8$) for G1107D PMCA3*a* ($P < 0.01$); 0.65 ± 0.03 ($n = 8$) for wt PMCA3*b* and 0.84 ± 0.04 ($n = 7$) for the G1107D PMCA3*b* ($P < 0.005$)].

Bioinformatics Analysis and Protein Modeling. An impairing effect of the G1107D mutation on the interplay between CaM and its binding domain was predicted by all algorithms used [PolyPhen2, HumMut, and sort intolerant from tolerant (SIFT)]. Alignment of orthologous protein sequences by ClustalW2 revealed that the G1107 residue is fully conserved across species, from worms (*Caenorhabditis elegans*) to humans (Fig. 5*A*). Molecular modeling of the CaM-binding domain of the wt (Fig. 5*B*) and mutated PMCA3 (Fig. 5*C*) shows that in all of the possible rotamers explored, the mutation determined atomic clashes, e.g., in the interaction of the D of mutated PMCA3 with L112 and E114 residues of CaM. It would be plausible to expect that the defective interaction of the two residues would unfavorably affect the interaction between the pump and CaM.

Discussion

Congenital ataxias (CAs) account for about 10% of nonprogressive infantile encephalopathies (19, 20). They are characterized by severe neonatal hypotonia and motor delay, followed by cerebellar ataxia in the first years of life. They are generally classified into pure cerebellar and syndromic forms (21), and their inheritance can be autosomal recessive (22), autosomal dominant (23, 24), or X-linked recessive (25, 26). Except for Joubert and related syndromes, which are caused by dysfunction in ciliary and centrosomal proteins (reviewed in ref. 27), the physiopathological mechanisms responsible for CAs are elusive. The genetic defect in *PMCA3* described here extends the disease phenotypes caused by PMCA defects to the area of X-linked cerebellar congenital ataxias. Both the unspliced variant *b* and the C-terminally truncated *a* variant of PMCA3 are abundant in human cerebellum (and brain), where they are widely expressed in the main (PF-PN) cerebellar synapse and where they play a critical role in PN and granular neurons Ca^{2+} homeostasis (28). As mentioned above, reduced Ca^{2+} influx has been reported in the PNs of an ataxic mouse (7, 8) and has been claimed to exacerbate the severity of other ataxic models (29). An ataxic phenotype (see above) has also been induced by the ablation of the PMCA2 gene in mice (12). However, no gene defects of Ca^{2+} ATPases (or of other Ca^{2+} transporters) had been reported to date in human ataxias. The results described here have documented decreased Ca^{2+} extrusion by the mutated PMCA3 pump expressed in model cell, particularly

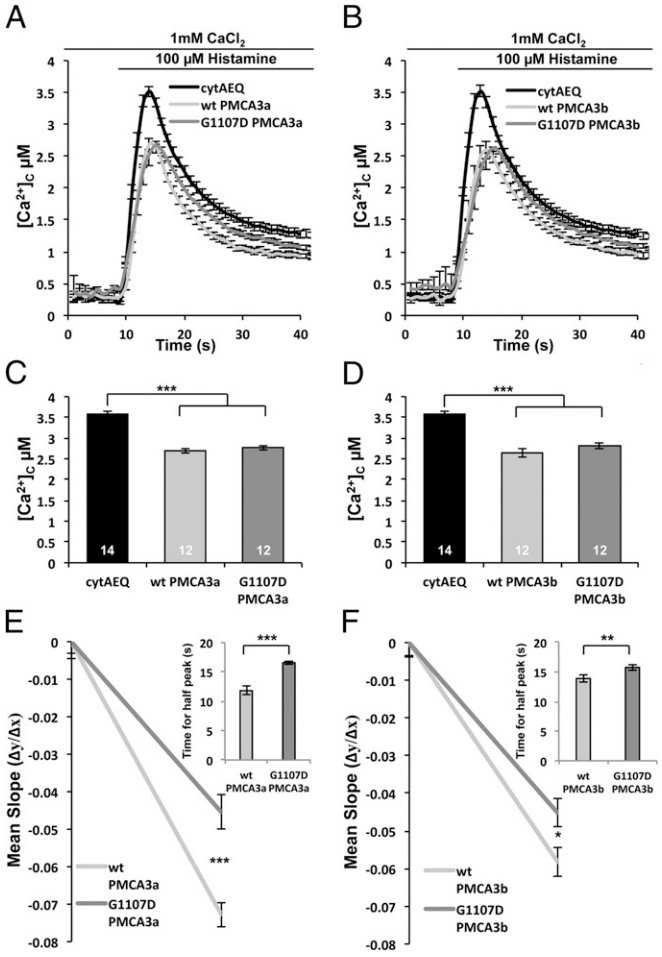

Fig. 3. Cytosolic Ca^{2+} measurements in HeLa cells overexpressing the wt and the mutant PMCA3 isoforms. Cells were cotransfected with cytAEQ and the expression plasmid for the *a* (*A*) or the *b* (*B*) wt, as well as mutated, PMCA3 variants. Cytosolic Ca^{2+} transients (*A* and *B*) were recorded following histamine stimulation, and the average peak values (*C* and *D*), as well as the mean slope of Ca^{2+} transients, were calculated at the half time of the peak decay (*E* and *F*). *Insets* in *E* and *F* show histograms representing the half time of the peak decay of Ca^{2+} transients. Bars in *C* and *D* represent mean $[Ca^{2+}]$ values upon stimulation (μM ± SEM). Bars in the *Insets* represent mean time for half-peak (seconds ± SEM). The traces and the histograms were obtained by averaging 15 independent experiments for each condition. $***P < 0.001$; $**P < 0.01$; $*P \leq 0.05$.

in its truncated version. The mutant pumps had the same ability of the wt pump to dispose of a suddenly incoming large Ca^{2+} pulse generated by the opening of the $InsP_3$ channels, but the defect became evident when the concentration of Ca^{2+} in the environment declined: at this point, the mutant pumps became clearly inadequate. A pattern of defect was also detected in the control of Ca^{2+} entering the cell from the external medium via the SOCE channels. In this case, a difference between the wt and the mutated PMCA pump was detected in the peak height of the Ca^{2+} transient and not in the decay phase from it. The difference in the peak height could have been attributable to the fact that the rate of Ca^{2+} entering through the SOCE channels was slower than that of the release of Ca^{2+} from the ER, making differences in the mutants visible. Alternatively, the handling of the Ca^{2+} that had entered through the plasma membrane could have been preferentially affected by PMCA pump close to the entry point, making differences better visible. The finding that no difference was detected in the decay phase of the second Ca^{2+} transient could be explained by the fact that pump-unrelated Ca^{2+} dissipation (e.g., by buffering and diffusion) would depend on the height of the peak transients; therefore, possible differences could have been masked by the increased rate of dissipation (in the first phase of the decay) in cell expressing the mutant pump. A difference was instead appreciated in the resting Ca^{2+} values at the end of transients.

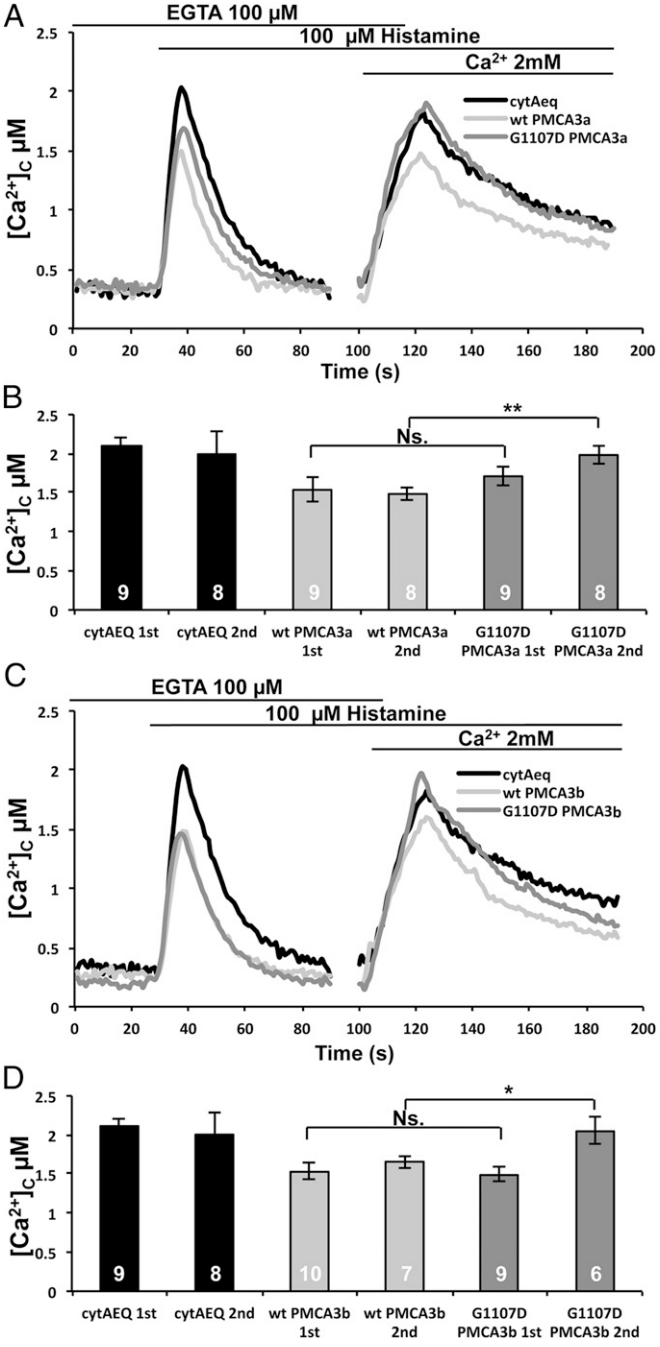

Fig. 4. Effect of the truncated (*A* and *B*) and full-length (*C* and *D*) wt and mutant pump on the ER Ca^{2+} mobilization and on the Ca^{2+} influx from the extracellular ambient. HeLa cells were cotransfected with cytAEQ and the PMCA3 constructs or transfected with cytAEQ only, perfused in KRB/EGTA buffer, and stimulated with histamine to release Ca^{2+} from the intracellular stores (first peak). Then, the perfusion medium was switched to KRB/Ca^{2+} (in the continuous presence of histamine) to stimulate Ca^{2+} entry from the extracellular ambient (second peak). The Ca^{2+} transients in *A* are those for the PMCA3*a* isoform, and the Ca^{2+} transients in *C* are those for the *b* variant. They are representative of at least six independent experiments. *B* and *D* show the averaged peak $[Ca^{2+}]$ values obtained upon stimulation. Bars represent means ± SEM obtained by averaging the values obtained in six independent experiments for each condition. $**P < 0.01$; $*P \leq 0.05$. Ns., not significant.

GENETICS

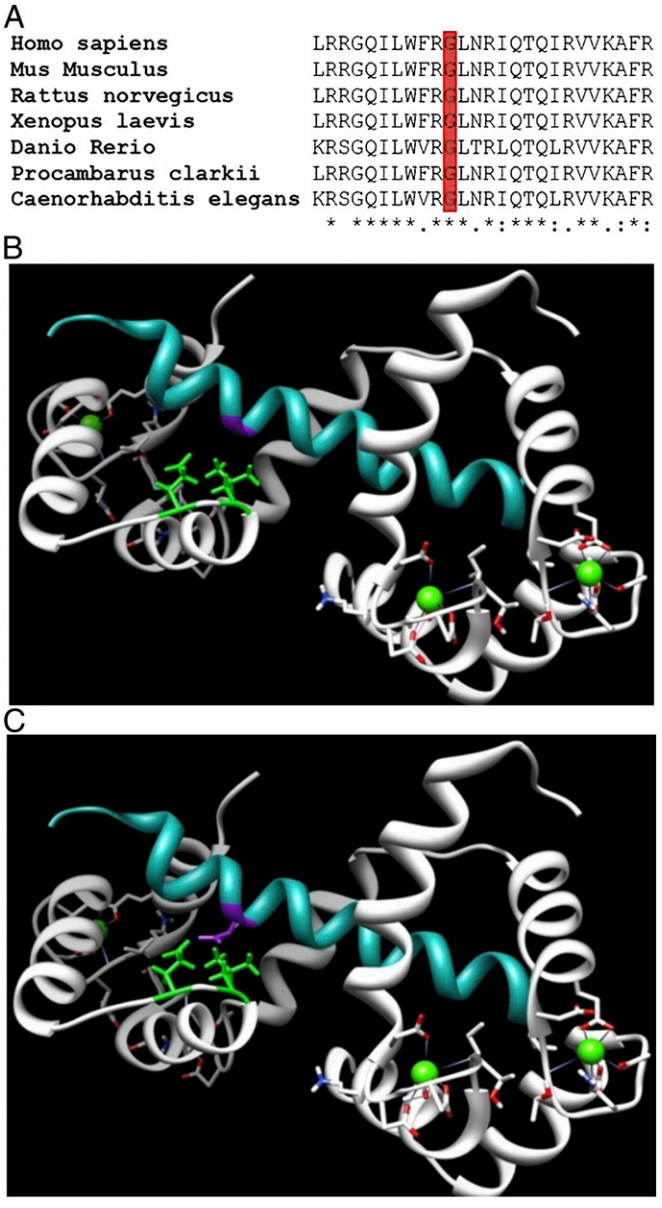

Fig. 5. Protein sequence alignment of human PMCA3 with its orthologs and molecular modeling of the interaction of the wt or mutated CaM-binding domain of PMCA and CaM. (*A*) Only the sequence around the variants p.G1107D in PMCA3 (highlighted in red) is shown. The p.G1107 residue is evolutionarily conserved throughout species. (*B*) The NMR structure of human PMCA4 CaM binding domain (PDB code 2KNE), which shares 100% sequence identity to the CaM-binding domain of human PMCA3, was used as a template (cyan helix). The p.G1096 residue, corresponding to p.G1107 of PMCA3, is highlighted in magenta. (*C*) Molecular model of mutated CaM-binding domain with substitution of glycine (G) with aspartic acid (D). As calculated by UCSF Chimera, all rotamers of the aspartic side (D) chain create atomic clashes [i.e., unfavorable interactions, with CaM (gray helix), in particular with residues L112 and E114 (in green)].

The decreased ability of the mutated pump to extrude Ca^{2+} could be conveniently ascribed to the impaired interplay of its binding domain with CaM. The suggestion is supported by the bioinformatic modeling of Fig. 5, which shows that the interaction between CaM and the mutated binding domain, is predicted to be looser because of the presence of the mutated Asp. The mutation would presumably reduce the ability of CaM to interact with its binding domain; i.e., the defect would tend to depress the basal activity of the pump. However, mutations of residues in the immediate vicinity of G1107 [i.e., W1093 to A (30)] or of D1080 to various residues (31) have, instead, been found to increase the basal activity of other pump isoforms. In these cases, the effect could have been attributable to a decreased autoinhibitory interaction of the CaM-binding domain with the main body of the pump. In principle, such an effect could have also been expected by the G1107D mutation; i.e., the situation generated by the mutation on the Ca^{2+} pumping function of PMCA3 is likely to be more complex. It could also be mentioned that, aside from their function in controlling basal Ca^{2+} levels, PMCAs are emerging as signaling molecules (32) and could be directly involved in local Ca^{2+} signaling through their interaction with Caveolin-1 (33) and in the regulation of the cytoskeleton through their interaction with 14-3-3 proteins (34, 35) or other interacting proteins (for a review, see ref. 1). More than a dozen X-linked gene defects generate a cerebellar phenotype (36), with those associated with mutations in the synaptic proteins oligophrenin-1 (*OPHN1*) (37, 38) and calcium/calmodulin-dependent serin protein kinase (*CASK*) (39, 40) being well-characterized. The CASK syndrome is caused by the disruption of the gene for the Ca^{2+}-CaM–dependent protein kinase, and it may be significant that CASK interacts through its PDZ [Post synaptic density protein (PSD95), Drosophila disc large tumor suppressor (Dlg1), and Zonula occludens-1 protein (zo-1)]-binding domain with the C terminal of the PMCA pump (41). PMCAs are part of a postsynaptic complex formed by metabotropic glutamate receptors (mGluR1), Homer (which interacts with OPHN1), and $InsP_3$ type 1 receptors ($InsP_3R1$) (42–44). The levels of mGluR1 and $InsP_3R1$ are reduced in PNs in several mouse models of ataxia, and it is interesting that late-onset human degenerative ataxias with a pure cerebellar phenotype have been related to the disruption of Ca^{2+}- and $InsP_3R$-dependent signaling pathways (45). The importance of maintaining the homeostasis of Ca^{2+} within neurons with exquisitely controlled precision may explain why a relatively mild defect in the extrusion ability of the PMCA3 pump could generate a severe neuronal (cerebellar) phenotype. The possible inability of the mutant pump to engage in functional multiprotein complexes handling synaptic Ca^{2+} nanodomains could be an additional factor in the cerebellar disease phenotype.

Materials and Methods

X-Exome Sequencing. Genomic DNA (3 μg) from the index patient (III:1 in Fig. 1) was used for constructing a single-end Illumina sequencing library using the Illumina Genomic DNA Single End Sample Prep kit, according to the instructions of the manufacturer. X-chromosome exome enrichment was performed for the sequencing library using the Agilent SureSelect Human X Chromosome Kit, which contains 47,657 RNA baits for 7,591 exons of the human X chromosome. Single-end deep sequencing was performed on the Illumina Genome Analyzer GAIIx. Read-length was 76 nt. Sequences were analyzed with in-house–developed tools. Nucleotide changes identified by NGS and segregation analysis in the family were confirmed by conventional sequencing using gene-specific primers.

Site-Directed Mutagenesis of Full-Length and Truncated Variants of hPMCA3 G1107D Mutant. Both PMCA3*b* (full-length) and PMCA3*a* (truncated*)* cDNAs of human origin were used as targets, and site-directed mutagenesis was performed according to the standard protocol of the manufacturer (Stratagene). The following primers were used: G1107D, 5′-ATCCTCTGGTTCCGGGACCTGAACCGGATTCAGACGC-3′ (forward); G1107D, 5′-GCGTCTGAATCCGGTTCAGGTCCCGGAACCAGAGGAT-3′ (reverse). All of the constructs were verified by sequencing.

Immunolocalization of the Overexpressed Pumps. HeLa cells were grown in DMEM high-glucose medium supplemented with 10% (vol/vol) FCS onto 13-mm glass coverslips. Transfection with 4 μg of total plasmid DNA was carried out with a Ca^{2+}-phosphate procedure. Thirty-six hours after transfection, the cells were washed twice with PBS [140 mM NaCl, 2 mM KCl, 1.5 mM KH_2PO_4, 8 mM Na_2HPO_4 (pH 7.4)], fixed for 20 min in 3.7% formaldehyde and washed three times with PBS. The cells were then permeabilized in 0.1% Triton X-100 in PBS, followed by a 1-h wash with 1% gelatin (type IV, from calf skin) in PBS and incubated for 1 h at 37 °C in a wet chamber with the 5F10 monoclonal Antibody (Affinity BioReagents) at a 1:100 dilution in PBS. Staining was carried out with Alexa Fluor 488–labeled anti-mouse secondary antibody (Molecular Probes) at a 1:50 dilution in PBS. After each incubation, cells were washed four times with PBS.

Fluorescence was analyzed with an Axiovert microscope (Zeiss) equipped with an AxioCam HRm camera (Zeiss). Images were acquired with AxioVision version 30 software (Zeiss).

Western Blotting Analysis. Forty-eight hours after transfection, HeLa cells were washed on ice with Ca^{2+}/Mg^{2+}-free phosphate buffer (Euroclone), followed by lysis in 50 mM Hepes, 150 mM NaCl, 1% Nonidet P-40, 1% sodium deoxycholate (pH 7.4) containing a protease inhibitor mixture (Sigma) for 10 min on ice. Postnuclear supernatants were collected after spinning for 10 min at 0.8 × *g*. Samples for electrophoresis were prepared in Sample Buffer supplemented with DTT (final concentration 100 mM) and urea (125 mg/mL) and incubated for 10 min at 37 °C. The total protein content was determined by the Bradford assay (Bio-Rad). Samples were loaded on a 8% SDS/PAGE Tris-HCl gel, transferred onto PVDF membranes (Bio-Rad), blocked for 1 h at room temperature using 5% nonfat dried milk (NFDM) in TBST [20 mM Tris-HCl (pH 7.4), 150 mM NaCl, 0.05% Tween-20] and incubated overnight with the specific primary antibody at 4 °C. Primary antibody anti-PMCA3 (1:1,000; Thermo Scientific), monoclonal anti-PMCA clone 5F10 (1:1,000; Thermo Scientific), and monoclonal anti–β-actin (1:30,000; Sigma) were used.

Aequorin Ca^{2+} Measurements. Transfected cytAEQ was reconstituted by incubating HeLa cells for 1–3 h with 5 μM coelenterazine in DMEM supplemented with 1% FBS at 37 °C and 5% CO_2. Additions to the Krebs–Ringer buffer (KRB) medium are specified in the figure legends. Measurements and calibration of aequorin signal were performed as previously described (15). Data are reported as means ± SEM. Statistical differences were evaluated by Student's two-tailed *t* test for unpaired samples. A *P* value of ≤0.05 was considered statistically significant.

Bioinformatic Analysis. To predict whether the missense variant was deleterious, we used the combined results of three different computer algorithms: SIFT (available at http://sift.jcvi.org), the polymorphism phenotyping program PolyPhen, (http://genetics.bwh.harvard.edu/pph); and PMut (available at http://mmb2.pcb.ub.es:8080/PMut). For evolutionary conservation, the protein sequences were downloaded from NCBI (http://www.ncbi.nlm.nih.gov/protein), and the alignments were calculated using ClustalW (http://www.ebi.ac.uk/clustalw2).

Protein Modeling. The structural model of the mutant and wt CaM-binding domain of human PMCA3 (NCBI accession no. NP_001001344.1) was derived by homology modeling using University of California at San Francisco (UCSF) Chimera modeling system (46). The NMR solution structure of the human PMCA4 bound to CaM [Protein Data Bank (PDB) code 2KNE], which shares 100% sequence identity to the CaM-binding domain of human PMCA3 was used as a template. The quality and stereochemistry of the model was assessed using ProSA-II (https://prosa.services.came.sbg.ac.at).

ACKNOWLEDGMENTS. We thank Dr. Rosalba Carrozzo and Prof. Charles Schwartz for help and advice, Melanie Bienek and Corinna Jensen for NGS, and Stefan Haas for help with NGS data analysis. This work was supported by grants from the Italian Telethon Foundation [Projects 492/B (to G.Z.) and GGP08145 (to E.B.)]; the Italian Ministry of University and Research (PRIN 2008) and the University of Padova (Progetto di Ateneo 2008 CPDA082825) (to M.B.); and Fondazione Cariparo (Progetti di Eccellenza 2008-2009) and ERA-Net Neuron (Grant nEUROsyn 2008) (to E.C.).

1. Brini M, Carafoli E (2009) Calcium pumps in health and disease. *Physiol Rev* 89:1341–1378.
2. Falchetto R, Vorherr T, Brunner J, Carafoli E (1991) The plasma membrane Ca2+ pump contains a site that interacts with its calmodulin-binding domain. *J Biol Chem* 266: 2930–2936.
3. Falchetto R, Vorherr T, Carafoli E (1992) The calmodulin-binding site of the plasma membrane Ca2+ pump interacts with the transduction domain of the enzyme. *Protein Sci* 1:1613–1621.
4. Kip SN, et al. (2006) Changes in the expression of plasma membrane calcium extrusion systems during the maturation of hippocampal neurons. *Hippocampus* 16:20–34.
5. Burette A, Weinberg RJ (2007) Perisynaptic organization of plasma membrane calcium pumps in cerebellar cortex. *J Comp Neurol* 500:1127–1135.
6. Eakin TJ, Antonelli MC, Malchiodi EL, Baskin DG, Stahl WL (1995) Localization of the plasma membrane Ca(2+)-ATPase isoform PMCA3 in rat cerebellum, choroid plexus and hippocampus. *Brain Res Mol Brain Res* 29:71–80.
7. Walter JT, Alviña K, Womack MD, Chevez C, Khodakhah K (2006) Decreases in the precision of Purkinje cell pacemaking cause cerebellar dysfunction and ataxia. *Nat Neurosci* 9:389–397.
8. Alviña K, Khodakhah K (2010) KCa channels as therapeutic targets in episodic ataxia type-2. *J Neurosci* 30:7249–7257.
9. Schultz JM, et al. (2005) Modification of human hearing loss by plasma-membrane calcium pump PMCA2. *N Engl J Med* 352:1557–1564.
10. Ficarella R, et al. (2007) A functional study of plasma-membrane calcium-pump isoform 2 mutants causing digenic deafness. *Proc Natl Acad Sci USA* 104:1516–1521.
11. Inoue Y, Matsumura Y, Inoue K, Ichikawa R, Takayama C (1993) Abnormal synaptic architecture in the cerebellar cortex of a new dystonic mutant mouse, Wriggle Mouse Sagami. *Neurosci Res* 16:39–48.
12. Empson RM, Turner PR, Nagaraja RY, Beesley PW, Knöpfel T (2010) Reduced expression of the Ca(2+) transporter protein PMCA2 slows Ca(2+) dynamics in mouse cerebellar Purkinje neurones and alters the precision of motor coordination. *J Physiol* 588:907–922.
13. Bertini E, et al. (2000) X-linked congenital ataxia: A clinical and genetic study. *Am J Med Genet* 92:53–56.
14. Li Y, et al. (2010) Resequencing of 200 human exomes identifies an excess of low-frequency non-synonymous coding variants. *Nat Genet* 42:969–972.
15. Brini M, et al. (1995) Transfected aequorin in the measurement of cytosolic Ca2+ concentration ([Ca2+]c). A critical evaluation. *J Biol Chem* 270:9896–9903.
16. Brini M, et al. (2003) A comparative functional analysis of plasma membrane Ca2+ pump isoforms in intact cells. *J Biol Chem* 278:24500–24508.
17. Brini M, Bano D, Manni S, Rizzuto R, Carafoli E (2000) Effects of PMCA and SERCA pump overexpression on the kinetics of cell Ca(2+) signalling. *EMBO J* 19:4926–4935.
18. Giacomello M, et al. (2011) Mutations in PMCA2 and hereditary deafness: A molecular analysis of the pump defect. *Cell Calcium* 50:569–576.
19. Sanner G, Hagberg B (1974) 188 cases of non-progressive ataxic syndromes in childhood. Aspects of aetiology and classification. *Neuropadiatrie* 5:224–235.
20. Esscher E, Flodmark O, Hagberg G, Hagberg B (1996) Non-progressive ataxia: Origins, brain pathology and impairments in 78 swedish children. *Dev Med Child Neurol* 38:285–296.
21. Steinlin M (1998) Non-progressive congenital ataxias. *Brain Dev* 20:199–208.
22. Guzzetta F, Mercuri E, Bonanno S, Longo M, Spanò M (1993) Autosomal recessive congenital cerebellar atrophy. A clinical and neuropsychological study. *Brain Dev* 15:439–445.
23. Imamura S, Tachi N, Oya K (1993) Dominantly inherited early-onset non-progressive cerebellar ataxia syndrome. *Brain Dev* 15:372–376.
24. Jen JC, Lee H, Cha YH, Nelson SF, Baloh RW (2006) Genetic heterogeneity of autosomal dominant nonprogressive congenital ataxia. *Neurology* 67:1704–1706.
25. Bruyn GW, Vianney De Jong JMB (1991) X-linked recessive ataxia. *Hereditary Neuropathies and Spinocerebellar Atrophies,* Handbook of Clinical Neurology, eds Vinken PJ, Bruyn GW (Elsevier, Amsterdam), pp 635–642.
26. Zanni G, et al. (2008) X-linked congenital ataxia: A new locus maps to Xq25-q27.1. *Am J Med Genet A* 146A:593–600.
27. Brancati F, Dallapiccola B, Valente EM (2010) Joubert Syndrome and related disorders. *Orphanet J Rare Dis* 5:20.
28. Carlson KM, Andresen JM, Orr HT (2009) Emerging pathogenic pathways in the spinocerebellar ataxias. *Curr Opin Genet Dev* 19:247–253.
29. Vig PJ, Subramony SH, McDaniel DO (2001) Calcium homeostasis and spinocerebellar ataxia-1 (SCA-1). *Brain Res Bull* 56:221–225.
30. Penheiter AR, Caride AJ, Enyedi A, Penniston JT (2002) Tryptophan 1093 is largely responsible for the slow off rate of calmodulin from plasma membrane Ca2+ pump 4b. *J Biol Chem* 277:17728–17732.
31. Pászty K, et al. (2002) Asp1080 upstream of the calmodulin-binding domain is critical for autoinhibition of hPMCA4b. *J Biol Chem* 277:36146–36151.
32. Brini M (2009) Plasma membrane Ca(2+)-ATPase: From a housekeeping function to a versatile signaling role. *Pflugers Arch* 457:657–664.
33. Daniel EE, El-Yazbi A, Cho WJ (2006) Caveolae and calcium handling, a review and a hypothesis. *J Cell Mol Med* 10:529–544.
34. Linde CI, et al. (2008) Inhibitory interaction of the 14-3-3 proteins with ubiquitous (PMCA1) and tissue-specific (PMCA3) isoforms of the plasma membrane Ca2+ pump. *Cell Calcium* 43:550–561.
35. Rimessi A, et al. (2005) Inhibitory interaction of the 14-3-3epsilon protein with isoform 4 of the plasma membrane Ca(2+)-ATPase pump. *J Biol Chem* 280:37195–37203.
36. Zanni G, Bertini ES (2011) X-linked disorders with cerebellar dysgenesis. *Orphanet J Rare Dis* 6:24.
37. Billuart P, et al. (1998) Oligophrenin-1 encodes a rhoGAP protein involved in X-linked mental retardation. *Nature* 392:923–926.
38. Zanni G, et al. (2005) Oligophrenin 1 mutations frequently cause X-linked mental retardation with cerebellar hypoplasia. *Neurology* 65:1364–1369.
39. Najm J, et al. (2008) Mutations of CASK cause an X-linked brain malformation phenotype with microcephaly and hypoplasia of the brainstem and cerebellum. *Nat Genet* 40:1065–1067.
40. Hsueh YP (2009) Calcium/calmodulin-dependent serine protein kinase and mental retardation. *Ann Neurol* 66:438–443.
41. Schuh K, Uldrijan S, Gambaryan S, Roethlein N, Neyses L (2003) Interaction of the plasma membrane Ca2+ pump 4b/CI with the Ca2+/calmodulin-dependent membrane-associated kinase CASK. *J Biol Chem* 278:9778–9783.
42. Sandonà D, Scolari A, Mikoshiba K, Volpe P (2003) Subcellular distribution of Homer 1b/c in relation to endoplasmic reticulum and plasma membrane proteins in Purkinje neurons. *Neurochem Res* 28:1151–1158.
43. Govek EE, et al. (2004) The X-linked mental retardation protein oligophrenin-1 is required for dendritic spine morphogenesis. *Nat Neurosci* 7:364–372.
44. Sgambato-Faure V, Xiong Y, Berke JD, Hyman SE, Strehler EE (2006) The Homer-1 protein Ania-3 interacts with the plasma membrane calcium pump. *Biochem Biophys Res Commun* 343:630–637.
45. Schorge S, van de Leemput J, Singleton A, Houlden H, Hardy J (2010) Human ataxias: A genetic dissection of inositol triphosphate receptor (ITPR1)-dependent signaling. *Trends Neurosci* 33:211–219.
46. Pettersen EF, et al. (2004) UCSF Chimera—a visualization system for exploratory research and analysis. *J Comput Chem* 25:1605–1612.

Supporting Information

Zanni et al. 10.1073/pnas.1207488109

SI Materials and Methods

Fibroblast Preparation. Primary fibroblast cultures were established from skin biopsy of individual II:1 (affected maternal uncle) and control. Skin biopsies were performed following written, informed consent, according to the rules of the Ethics Committee of the Ospedale Pediatrico Bambino Gesù (OPBG). Fibroblasts were cultured in DMEM/high glucose (EuroClone) at 37 °C. At confluence, cells were detached from the flasks with trypsin/EDTA (Sigma-Aldrich) and subcultured at the same density.

RT-PCR Analysis of the Splicing Variants of the Human PMCA3*a* and -*b* Transcript and Analysis of Ca^{2+}-Exporting Activity in Patient-Derived Fibroblasts. A semiquantitative RT-PCR analysis of the *b* and the *a* splicing variants of the PMCA3 transcript was performed in control and in patient-derived fibroblasts. Human fetal and adult brain, as well as cerebellum, were used as positive controls.

Total RNA from skin fibroblasts of the patient was isolated using TRIzol solution (Invitrogen), according to the protocol of the manufacturer. RNA from human brain and cerebellum was obtained from Clontech. One microgram of each RNA sample was reverse-transcribed with the SuperScript First-Strand Synthesis system and random hexamers as primers (Invitrogen Life Technologies). The following primers were used: *b* variant, 5′-CTCTGGTTCCGGGGCCTG-3′ (forward) and 5′-TTAGAGGACGTCTCCACGCT-3′ (reverse); *a* variant, 5′-CTCTGGTTCCGGGGCCTG-3′ (forward) and 5′-CTACGGAACGCTTTCACCACC-3′ (reverse). They were expected to amplify a 510-nt fragment in the case of *b* variant and a 205-nt fragment in the case of PMCA3*a* variant. As shown in Fig. S1*A*, fibroblasts express much lower levels of the PMCA3*b* transcript, and undetectable levels of that of the PMCA3*a*, in comparison with brain and cerebellar neurons.

Even if it seemed unlikely that these small amounts of the PMCA3 pump would have a significant role in the homeostasis of Ca^{2+} in the fibroblasts, we still considered it useful to perform some experiments on their Ca^{2+} homeostasis. The Ca^{2+}-handling ability of the PMCA3 pump was monitored in control and patient-derived fibroblasts transfected with the plasmid encoding the Ca^{2+}-sensing probe aequorin targeted to the cytoplasm [cytAEQ (1)]. Cells were stimulated with the $InsP_3$-generating agonist histamine, and the Ca^{2+} transients were recorded. As shown in Fig. S1*B*, no differences in the Ca^{2+} transients kinetics and in the peak heights (Fig. S1*C*) were found between control and patient-derived fibroblasts [Fig. S1*C*; values in μM ± SEM were: 2.21 ± 0.03 (n = 26) for control fibroblasts; and 2.31 ± 0.04 (n = 29) for patient-derived fibroblasts].

Measurements of Resting Ca^{2+} Concentration in the ER and Effect of Stimulation in HeLa Cells Overexpressing the Different PMCA3 Constructs. Endoplasmic-reticulum targeted aequorin (erAEQ) was used to measure the intralumenal ER Ca^{2+} concentration (2). Functional aequorin was reconstituted with a modified prosthetic group, coelenterazine n, to decrease the affinity of the photoprotein and, thus, to monitor the high values of ER Ca^{2+} (3). In all experiments, erAEQ reconstitution was carried out after depleting the ER lumen of Ca^{2+} with 5 μM ionomycin as described previously (2). In the experiment shown in Fig. S2, parallel batches of HeLa cells, transfected with either erAEQ or co-transfected with erAEQ, and the different PMCA3 variants were first perfused with KRB supplemented with 1 mM $CaCl_2$ and then, when the plateau was reached, challenged with the $InsP_3$-generating agonist histamine. Independently of the PMCA3 variant used, cells overexpressing PMCA3 pumps exhibited a lower steady-state value of ER Ca^{2+} (first plateau): 343.6 ± 4 μM for wt PMCA3*a*; 315.4 ± 14.76 μM for G1107D PMCA3*a*; 352 ± 23 μM for wt PMCA3*b*; 317.2 ± 16.11 μM for G1107D PMCA3*b*; and 513.26 ± 20.32 μM for control cells ($P < 0.001$ and $P \leq 0.05$; Fig. S2 *A* and *B*). Possibly, the finding may help explain why our protocol failed to reveal effects of the PMCA3 mutation on the height of the peak transient generated by the release of Ca^{2+} from the ER. Possibly, under these conditions, the reduction of the ER Ca^{2+} level was dominant. Interestingly, PMCA-overexpressing cells also had a lower plateau value after histamine stimulation with respect to control cells, the differences being smaller in cells expressing the mutant pump than in those overexpressing the wt form. This suggests that the PMCA pump may have possibly lowered Ca^{2+} in the microdomains, available to the SERCA pump, thus affecting its ability to pump Ca^{2+} into the ER. The difference in ER Ca^{2+} after histamine stimulation (second plateau) in the cells overexpressing the mutated pump would suggest its lower ability to affect the activity of the SERCA pump compared with the wt pump and thus, indirectly, to extrude Ca^{2+} form the cell. The defect is evident in the PMCA3*a* variant.

1. Brini M, et al. (1995) Transfected aequorin in the measurement of cytosolic Ca2+ concentration ([Ca2+]c). A critical evaluation. *J Biol Chem* 270:9896–9903.
2. Montero M, et al. (1995) Monitoring dynamic changes in free Ca2+ concentration in the endoplasmic reticulum of intact cells. *EMBO J* 14:5467–5475.
3. Barrero MJ, Montero M, Alvarez J (1997) Dynamics of [Ca2+] in the endoplasmic reticulum and cytoplasm of intact HeLa cells. A comparative study. *J Biol Chem* 272: 27694–27699.

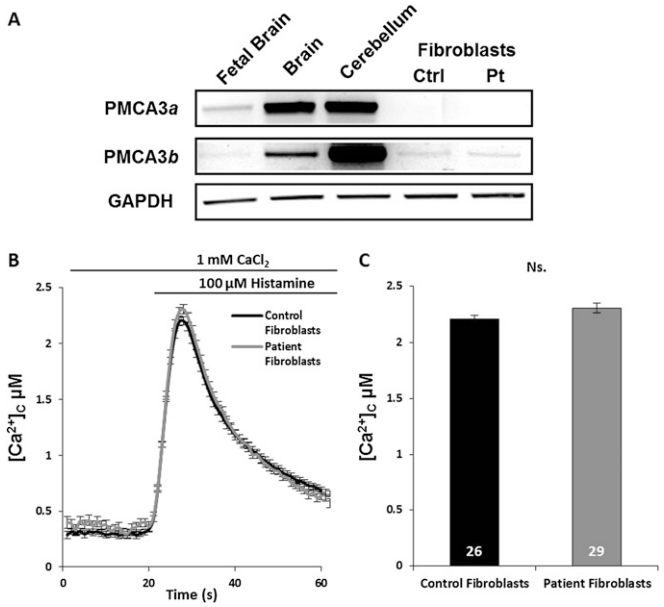

Fig. S1. Semiquantitative RT-PCR analysis of the full-length and truncated splicing variants of the human *PMCA3* transcript and analysis of intracellular Ca^{2+} handling in control vs. patient-derived fibroblasts. (*A*) Full-length and truncated splicing variants of the *PMCA3* transcript in human control fetal and adult brain, cerebellum, and control (Ctrl) vs. patient (Pt)-derived fibroblasts. GADPH is shown as a control. The expression of the splicing variants is weak or absent in fibroblasts and fetal brain. Cerebellum expresses the highest level of the full length PMCA3 variants, compared with brain. (*B* and *C*) Fibroblasts were transfected with cytAEQ and stimulated with histamine in a medium containing 1 mM $CaCl_2$, and cytosolic Ca^{2+} transients were recorded. (*B*) Kinetics of the Ca^{2+} transients in the two fibroblast batches. The traces are the average of 26 and 29 independent experiments performed in control or patient-derived fibroblasts, respectively. (*C*) Average of peak heights (means ± SEM). Ns. , not significant.

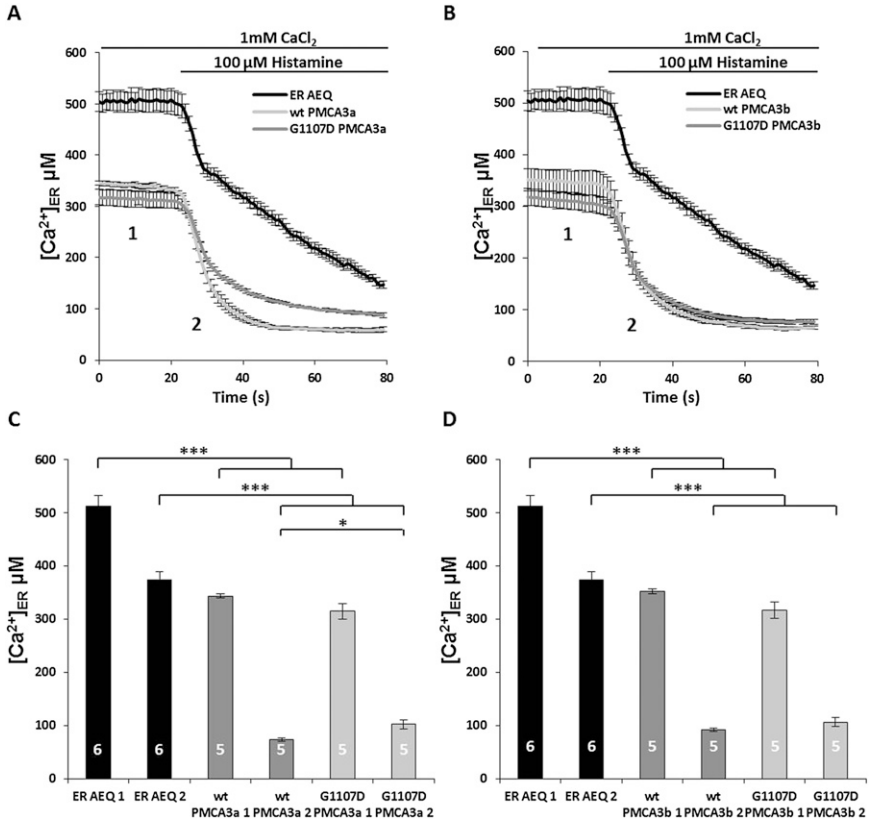

Fig. S2. Measurements of Ca^{2+} concentration in the lumen of ER, $[Ca^{2+}]_{er}$. HeLa cells were cotransfected with erAEQ (2) and the PMCA3 constructs or transfected with erAEQ only. Transfected HeLa cells were depleted of Ca^{2+} as described above and then incubated with 5 µM coelenterazine n in modified KRB supplemented with 600 µM EGTA. After extensive washing, the coverslip with the cells was placed in the thermostated chamber of the luminometer and perfused with KRB medium supplemented with 100 µM EGTA. Then, the EGTA was replaced with 1 mM $CaCl_2$ until a plateau was reached indicating the complete refilling of the lumen of the ER (1, first plateau). Then, the cells were challenged with the $InsP_3$-linked agonist histamine to induce the release of Ca^{2+} from the ER lumen, and the trace reached a second plateau level (2, second plateau). (*A* and *B*) ER Ca^{2+} levels and effects of the $InsP_3$-generating agonist histamine on it. The traces were obtained from the average of at least five independent experiments. (*C* and *D*) Bars represent the average plateau values of ER Ca^{2+} level before (1) and after (2) histamine stimulation in µM ± SEM. ***$P < 0.001$;*$P \leq 0.05$. The means were obtained from at least five independent experiments for each condition.